Hindawi
Journal of Nanomaterials
Volume 2018, Article ID 9063609, 9 pages
https://doi.org/10.1155/2018/9063609

Research Article

On the Stress Transfer of Nanoscale Interlayer with Surface Effects

Quan Yuan [1] **and Mengjun Wu** [2]

[1] *School of Architecture and Civil Engineering, Xihua University, Hongguang Town, Chengdu 610039, China*
[2] *China Merchants Chongqing Communications Research & Design Institute Co., Ltd., Chongqing 400067, China*

Correspondence should be addressed to Mengjun Wu; wumengjun@cmhk.com

Received 18 September 2017; Revised 7 December 2017; Accepted 14 December 2017; Published 17 January 2018

Academic Editor: Jim Low

An improved shear-lag model is proposed to investigate the mechanism through which the surface effect influences the stress transfer of multilayered structures. The surface effect of the interlayer is characterized in terms of interfacial stress and surface elasticity by using Gurtin–Murdoch elasticity theory. Our calculation result shows that the surface effect influences the efficiency of stress transfer. The surface effect is enhanced with decreasing interlayer thickness and elastic modulus. Nonuniform and large residual surface stress distribution amplifies the influence of the surface effect on stress concentration.

1. Introduction

Biomaterials and composites, such as nacre, bone, and ceramic, exhibit typical characteristics of a multilayered structure, which is composed of thick platelet-shaped hard phases and thin soft interlayers [1–4]. The discrete hard phases are bounded together but spaced from one another by the interlayers (adhesive layer). The volume fraction of interlayers is much smaller than the one of the large-scale hard phase in biomaterials. Interfaces of multilayered structure are coupled by those interlayers whose thicknesses have to shrink to microns or nanometers. For instance, the protein interlayer in nacre is about 20 nm thick; the matrix layer of bone and dentin is about 240 nm thick [3]. The robustness and stress transfer of the multilayered structure are ensured by the introduction of interlayers. The interlayer morphology determines the stress distribution and failure mode of structures under external forces [5, 6]. Classical shear-lag theory is based on some simple assumptions and continuity condition at the interfaces; this theory is used to effectively study stress distribution in a multilayered structure [6]. In shear-lag analysis, the interlayers are treated as macroscopic continuum matter, regardless of their thickness [2, 6]. Kotha et al. [2] and Tsai et al. [7] assumed that the interlayers only carry shear stress and are uniformly deformed with the stress field of the structure; when the interlayer thickness is reduced to the nanoscale level, the surface effects of the interlayers will influence the stress transfer of the multilayered structure because of the extremely large ratio of the surface area to the interlayer volume. However, the mechanism through which size and surface effects of the nanoscale interlayers influence stress transfer remains unclear.

Two main types of surface elasticity theory can characterize the surface effects for nanoscale objects [8]. The first type is the Gurtin–Murdoch elasticity model and its extension, in which the surface layer is considered as a membrane with vanishing thickness and assumed to perfectly adhere to the bulk substrate [9]. The Gurtin–Murdoch elasticity model has been used to analyze the natural frequency of microbeams [10], bridging mechanism of nanofibers [11], and near-tip stress fields [12]. Continuum quantities, surface free energy, and surface stress are central concepts in these analyses. Analogous to the bulk elastic constants, the introduced surface elastic constants are difficult to measure. An alternative choice of Eulerian surface-energy density is adopted to describe surface traction; the surface elastic constants are then no longer needed [13]. This improved surface elastic theory is further used to study the elastic properties of fcc metallic nanofilms under biaxial tension. The second type is the discrete Frenkel–Kontorova model [14], where the surface layer is represented by atoms connected together by

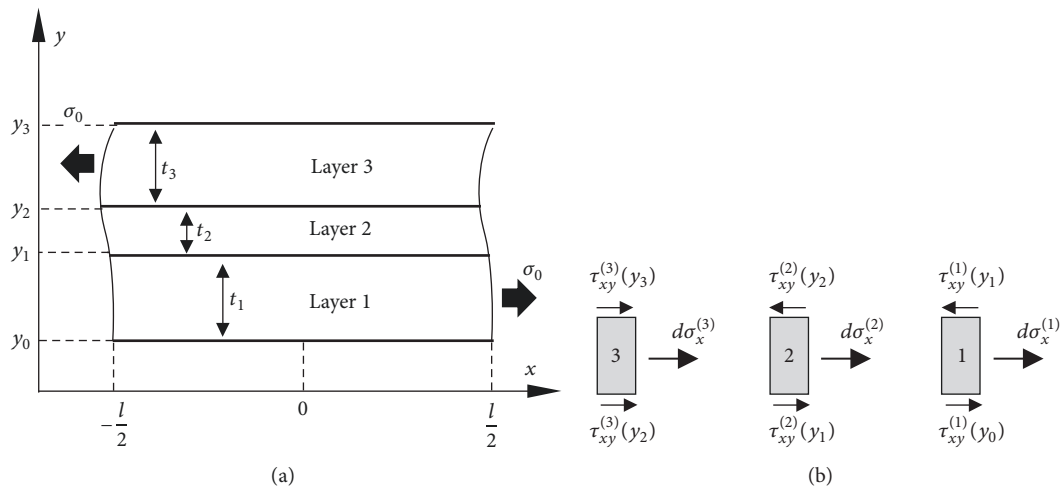

Figure 1: The geometry of multilayered structure.

springs or virtual bonds. The Frenkel–Kontorova model is used to calculate the surface stress of Cu(1, 1, 1) nanosheets [8]. The two types of surface elasticity model are both effective in describing the size-dependent mechanical properties of micro-/nanosized materials. Therefore, the macroscopic hard layers of multilayered structures comprise a considerable volume fraction and carry all external loads. The nanoscale interlayers dominate stress transfer, which results in the feasibility of applying the Gurtin–Murdoch model.

This study aims to elucidate the planar stress transfer mechanism of the nanoscale interlayers in a multilayered structure. Considering the geometry of the multilayered structure, the plane strain behavior of the hard layer subjected to tension is formulated using shear-lag theory. The surface effects of the interlayers at the interface coupled with stress transfer are formulated by the Gurtin–Murdoch model. Using the stress jump across the interface and the continuity condition of the interlayers, the global interfacial shear stress dominant governing equations are established. We obtain the stress distributions of the multilayered structure with three surface stress situations.

2. Shear-Lag Analysis of Interlayers with Surface Effects

2.1. Mathematical Formulation. As the main parts of a multilayered structure, hard layers are subjected to external load. The interlayers acting as adhesive layers strongly influence connection and stress transfer in the structure. We consider a simple sandwich laminate structure with one adhesive (layer 2) and two hard layers (layer 1 and layer 3) to estimate how the surface effects of the nanoscale interlayers influence stress transfer (Figure 1(a)). For hard layers, it seems reasonable to utilize approximate planar isotropy and emphasize the mechanical anisotropy along the thickness direction. In order to investigate the stress transfer under tension, the through-thickness normal strain and normal stress (y direction) are neglected according to Kamat et al.'s and Nairn and Mendels's shear-lag model (see [1, 6]). The thickness and elastic modulus of interlayers are much smaller than those of hard layers, and the macroscopic heterogeneity is neglected. The structure length is l, whereas the thicknesses of layers 1–3 are t_1, t_2, and t_3, respectively, where $t_2 \ll t_1, t_3$. Equilibrium tensions are forced on the right edge of layer 1 and left edge of layer 3. $S_1(y = y_1)$ and $S_2(y = y_2)$ are the upper and lower interfaces of the interlayer. The edges at $y = y_0$ and $y = y_3$ are free boundaries.

In the absence of body forces and under the condition of infinitesimal deformation, the geometric equations, constitutive relations, and equilibrium equations of every layer are as follows:

$$\varepsilon_x^{(i)} = \frac{\partial u^{(i)}}{\partial x}, \tag{1}$$

$$\varepsilon_y^{(i)} = \frac{\partial v^{(i)}}{\partial y}, \tag{2}$$

$$\gamma_{xy}^{(i)} = \frac{\partial u^{(i)}}{\partial y} + \frac{\partial v^{(i)}}{\partial x}, \tag{3}$$

$$\varepsilon_x^{(i)} = \frac{1}{E^{(i)}}\left[\sigma_x^{(i)} - \upsilon^{(i)}\sigma_y^{(i)}\right], \tag{4}$$

$$\varepsilon_y^{(i)} = \frac{1}{E^{(i)}}\left[\sigma_y^{(i)} - \upsilon^{(i)}\sigma_x^{(i)}\right], \tag{5}$$

$$\gamma_{xy}^{(i)} = \frac{\tau_{xy}^{(i)}}{G^{(i)}}, \tag{6}$$

$$\frac{\partial \sigma_x^{(i)}}{\partial x} + \frac{\partial \tau_{xy}^{(i)}}{\partial y} = 0, \tag{7}$$

$$\frac{\partial \tau_{xy}^{(i)}}{\partial x} + \frac{\partial \sigma_y^{(i)}}{\partial y} = 0, \tag{8}$$

where superscript "i" denotes the ith layer; (u, v), $(\varepsilon_x, \varepsilon_y, \gamma_{xy})$, and $(\sigma_x, \sigma_y, \tau_{xy})$ are the components of the displacement

vector, strain tensor, and stress tensor, respectively. $E^{(i)}$, $G^{(i)}$, and $v^{(i)}$ are the elastic modulus, shear modulus, and Poisson's ratio of the ith layer. For the infinitesimal sections of layers 1–3 (Figure 1(b)), equilibrium (7) is integrated along the thickness direction of every layer. We then obtain

$$t_1 \frac{d\overline{\sigma}_x^{(1)}}{dx} - \tau_{xy}^{(1)}(y_1) + \tau_{xy}^{(1)}(y_0) = 0, \tag{9}$$

$$t_2 \frac{d\overline{\sigma}_x^{(2)}}{dx} - \tau_{xy}^{(2)}(y_2) + \tau_{xy}^{(2)}(y_1) = 0, \tag{10}$$

$$t_3 \frac{d\overline{\sigma}_x^{(3)}}{dx} + \tau_{xy}^{(3)}(y_2) + \tau_{xy}^{(1)}(y_3) = 0, \tag{11}$$

where $\overline{(\,)}$ indicates averaging over the thickness of the ith layer, such as

$$\overline{\sigma}_x^{(i)} = \frac{1}{t_i}\int_{y_{i-1}}^{y_i} \sigma_x^{(i)} dy, \tag{12}$$

which represents the normal stress of the ith layer. $\tau_{xy}^{(i)}(y_i)$ and $\tau_{xy}^{(i)}(y_{i-1})$ are the interfacial shear stress at the upper and lower interfaces of the interlayer.

Substituting (1) into (4) and averaging the thickness of the ith layer provide

$$\frac{d\overline{u}^{(i)}}{dx} = \frac{1}{E^{(i)}}\left[\overline{\sigma}_x^{(i)} - v^{(i)}\overline{\sigma}_y^{(i)}\right]. \tag{13}$$

For stress transfer problems during loading in the x direction, $\overline{\sigma}_y^{(i)}$ can be eliminated. Equation (13) is reduced to 1D Hooke's law as follows:

$$\frac{d\overline{u}^{(i)}}{dx} = \frac{1}{E^{(i)}}\overline{\sigma}_x^{(i)}. \tag{14}$$

Tsai et al. have performed experimental analysis to verify the nonlinear deformation and adhesive stress distribution of interlayers in joints [7]. For the isotropic and unidirectional laminated structure, the transferred force is not altered by the interlayers with relatively low shear modulus and thickness. An appropriate assumption about interlayers has been used in Nairn's planar shear-lag analysis which is employed in this paper. Assuming that the shear stress in each layer is a linear distribution along the thickness, the shear stress in the ith layer can be written as follows:

$$\tau_{xy}^{(i)}(y) = \left(1 - \frac{y - y_{i-1}}{t_i}\right)\tau_{xy}^{(i)}(y_{i-1}) + \frac{y - y_{i-1}}{t_i}\tau_{xy}^{(i)}(y_i). \tag{15}$$

We need to introduce the general shear-lag assumption, $\partial v^{(i)}/\partial x$, to proceed. Equation (3) can be simplified as $\gamma_{xy}^{(i)} = \partial u^{(i)}/\partial y$. Combining (6) and (15) provides

$$\frac{\partial u^{(i)}}{\partial y} = \frac{1}{G^{(i)}}\left[\left(1 - \frac{y - y_{i-1}}{t_i}\right)\tau_{xy}^{(i)}(y_{i-1}) + \frac{y - y_{i-1}}{t_i}\tau_{xy}^{(i)}(y_i)\right]. \tag{16}$$

Equation (16) is averaged over the thickness of each layer by using the transform method proposed by McCartuay and developed by Nairn and then expressed as follows [6]:

$$\overline{u}^{(1)} = u^{(1)}(y_1) + \frac{t_1}{6G^{(1)}}\tau_{xy}^{(1)}(y_0) + \frac{t_1}{3G^{(1)}}\tau_{xy}^{(1)}(y_1), \tag{17}$$

$$\overline{u}^{(2)} = u^{(2)}(y_1) - \frac{t_2}{3G^{(2)}}\tau_{xy}^{(2)}(y_1) + \frac{t_2}{6G^{(2)}}\tau_{xy}^{(2)}(y_2), \tag{18}$$

$$\overline{u}^{(2)} = -u^{(2)}(y_2) - \frac{t_2}{6G^{(2)}}\tau_{xy}^{(2)}(y_1) + \frac{t_2}{3G^{(2)}}\tau_{xy}^{(2)}(y_2), \tag{19}$$

$$\overline{u}^{(3)} = -u^{(3)}(y_2) - \frac{t_3}{3G^{(3)}}\tau_{xy}^{(3)}(y_2) + \frac{t_3}{6G^{(3)}}\tau_{xy}^{(3)}(y_3). \tag{20}$$

At the $S_1(y = y_1)$ and $S_2(y = y_2)$ interfaces, the boundary conditions of displacement continuity can be expressed as follows:

$$u^{(1)}(y_1) = u^{(2)}(y_1), \quad u^{(2)}(y_2) = u^{(3)}(y_2). \tag{21}$$

After subtracting (17) from (18) and (14) from (19), differentiating the differences with respect to x and using (21) lead to

$$\begin{aligned}\frac{d\overline{u}^{(1)}}{dx} - \frac{d\overline{u}^{(2)}}{dx} &= \frac{t_2}{3G_2}\frac{d\tau_{xy}^{(2)}(y_1)}{dx} - \frac{t_2}{6G_2}\frac{d\tau_{xy}^{(2)}(y_2)}{dx} + \frac{t_1}{6G_1}\frac{d\tau_{xy}^{(1)}(y_0)}{dx} + \frac{t_1}{3G_1}\frac{d\tau_{xy}^{(1)}(y_1)}{dx},\\ \frac{d\overline{u}^{(3)}}{dx} - \frac{d\overline{u}^{(2)}}{dx} &= -\frac{t_3}{3G_3}\frac{d\tau_{xy}^{(3)}(y_3)}{dx} + \frac{t_3}{6G_3}\frac{d\tau_{xy}^{(3)}(y_3)}{dx} + \frac{t_2}{6G_2}\frac{d\tau_{xy}^{(2)}(y_1)}{dx} - \frac{t_2}{3G_2}\frac{d\tau_{xy}^{(2)}(y_2)}{dx}.\end{aligned} \tag{22}$$

Noticing the stress jump cross the interface induced by surface effects, the equilibrium condition of the Gurtin–Murdoch elasticity model at S_1 and S_2 interfaces is written as follows [9–11]:

$$\langle\sigma_{nn}\rangle - \sigma_{\alpha\beta}^S\kappa_{\alpha\beta} = 0, \quad \langle t_\alpha\rangle + \sigma_{\alpha\beta,\beta}^S = 0, \tag{23}$$

where $\sigma_{\alpha\beta}^S$ represents the surface stresses; $\kappa_{\alpha\beta}$ is the interface curvature. $\langle\sigma_{nn}\rangle$ and $\langle t_\alpha\rangle$ denote the stress jump along the tangential and normal directions, respectively. For the plane interface $\kappa_{\alpha\beta} = 0$, no stress jump is found in the y direction.

Moreover, the surface stress at an isotropic interface can be provided as follows [9–11]:

$$\sigma_{\alpha\beta}^{S_i} = \vartheta_s^{(i)}\delta_{\alpha\beta} + 2\mu_s^{(i)}\varepsilon_{\alpha\beta} + \lambda_s^{(i)}\varepsilon_{\gamma\gamma}\delta_{\alpha\beta}, \tag{24}$$

where $\delta_{\alpha\beta}$ is the Kronecker delta. $\vartheta_s^{(i)}$ is the residual interface tension, and $\mu_s^{(i)}$ and $\lambda_s^{(i)}$ are the surface elastic constants. The surface stress at S_1 and S_2 interfaces can be expressed as follows using (4) and (5):

$$\sigma_x^{S_1} = \vartheta_s^{(1)} + \frac{2\mu_s^{(1)} + \left(1 - \upsilon^{(2)}\right)\lambda_s^{(1)}}{E^{(2)}}\frac{d\overline{\sigma}_{2x}}{dx}, \tag{25}$$

$$\sigma_x^{S_2} = \vartheta_s^{(2)} + \frac{2\mu_s^{(2)} + \left(1 - \upsilon^{(2)}\right)\lambda_s^{(2)}}{E^{(2)}}\frac{d\overline{\sigma}_{2x}}{dx}. \tag{26}$$

The tangential stress jump can be obtained by combining (23), (25), and (26) and using (6):

$$\tau_{xy}^{(2)}(y_1) - \tau_{xy}^{(1)}(y_1) = -\frac{d\sigma_x^{S_1}}{dx}, \tag{27}$$

$$\tau_{xy}^{(3)}(y_2) - \tau_{xy}^{(2)}(y_2) = \frac{d\sigma_x^{S_2}}{dx}. \tag{28}$$

The interlayer can be assumed to only carry shear stress because of the small thickness and stiffness [1–3] and $\overline{\sigma}_{2x}$ can be neglected. Substituting (25) and (26) into (27) and (28) and differentiating the two equations with respect to x lead to

$$\begin{aligned}\frac{d\tau_{xy}^{(1)}(y_1)}{dx} - \frac{d\tau_{xy}^{(2)}(y_1)}{dx} &= \frac{d^2\vartheta_s^{(1)}}{dx^2},\\ \frac{d\tau_{xy}^{(3)}(y_2)}{dx} - \frac{d\tau_{xy}^{(2)}(y_2)}{dx} &= \frac{d^2\vartheta_s^{(2)}}{dx^2}.\end{aligned} \tag{29}$$

Furthermore, the normal stress of the two hard layers can be deduced as follows by substituting (29) into (22) and then using (14):

$$\begin{aligned}\overline{\sigma}_x^{(1)} &= \frac{\left(t_1G^{(2)} + t_2G^{(1)}\right)E^{(1)}}{3G^{(1)}G^{(2)}}\frac{d\tau_{xy}^{(2)}(y_1)}{dx}\\ &\quad - \frac{t_2E^{(1)}}{6G^{(2)}}\frac{d\tau_{xy}^{(2)}(y_2)}{dx} + \frac{t_1E^{(1)}}{3G^{(1)}}\frac{d^2\vartheta_s^{(1)}}{dx^2},\\ \overline{\sigma}_x^{(3)} &= \frac{t_2E^{(3)}}{6G^{(2)}}\frac{d\tau_{xy}^{(2)}(y_1)}{dx}\\ &\quad - \frac{\left(t_2G^{(3)} + t_3G^{(2)}\right)E^{(3)}}{3G^{(2)}G^{(3)}}\frac{d\tau_{xy}^{(2)}(y_2)}{dx}\\ &\quad - \frac{t_3E^{(3)}}{3G^{(3)}}\frac{d^2\vartheta_s^{(2)}}{dx^2}.\end{aligned} \tag{30}$$

Solving (30), the interfacial shear stress at the upper and lower interlayer interfaces can be expressed as follows:

$$\begin{aligned}\frac{d\tau_{xy}^{(2)}(y_1)}{dx} &= \frac{2\left(t_2G^{(3)} + t_3G^{(2)}\right)E^{(3)}}{G^{(3)}X}\overline{\sigma}_x^{(1)} - \frac{t_2E^{(1)}}{X}\overline{\sigma}_x^{(3)}\\ &\quad - \frac{2\left(t_2G^{(3)} + t_3G^{(2)}\right)t_1E^{(1)}E^{(3)}}{3G^{(1)}G^{(3)}X}\frac{d^2\vartheta_s^{(1)}}{dx^2}\\ &\quad - \frac{t_2t_3E^{(1)}E^{(3)}}{3G^{(3)}X}\frac{d^2\vartheta_s^{(2)}}{dx^2},\end{aligned} \tag{31}$$

$$\begin{aligned}\frac{d\tau_{xy}^{(2)}(y_2)}{dx} &= \frac{t_2E^{(3)}}{X}\overline{\sigma}_x^{(1)} - \frac{2\left(t_1G^{(2)} + t_2G^{(1)}\right)E^{(1)}}{G^{(1)}X}\overline{\sigma}_x^{(3)}\\ &\quad - \frac{t_1t_2E^{(1)}E^{(3)}}{3G^{(1)}X}\frac{d^2\vartheta_s^{(1)}}{dx^2}\\ &\quad - \frac{2\left(t_1G^{(2)} + t_2G^{(1)}\right)t_3E^{(1)}E^{(3)}}{3G^{(1)}G^{(3)}X}\frac{d^2\vartheta_s^{(2)}}{dx^2},\end{aligned} \tag{32}$$

where $X = 2(t_1G^{(2)} + t_2G^{(1)})(t_2G^{(3)} + t_3G^{(2)})E^{(1)}E^{(3)}/3G^{(1)}G^{(2)}G^{(3)} - t_2^2E^{(1)}E^{(3)}/6G^{(2)}$.

Moreover, differentiating (9) with respect to x and using (27) and (31) lead to

$$\begin{aligned}\frac{d^2\overline{\sigma}_x^{(1)}}{dx^2} &= \frac{1}{t_1}\frac{d\tau_{xy}^{(1)}(y_1)}{dx}\\ &= \frac{2\left(t_2G^{(3)} + t_3G^{(2)}\right)E^{(3)}}{t_1G^{(3)}X}\overline{\sigma}_x^{(1)} - \frac{t_2E^{(1)}}{t_1X}\overline{\sigma}_x^{(3)}\\ &\quad + \left[\frac{1}{t_1} - \frac{2\left(t_2G^{(3)} + t_3G^{(2)}\right)E^{(1)}E^{(3)}}{3G^{(1)}G^{(3)}X}\right]\frac{d^2\vartheta_s^{(1)}}{dx^2}\\ &\quad - \frac{t_2t_3E^{(1)}E^{(3)}}{3t_1G^{(3)}X}\frac{d^2\vartheta_s^{(2)}}{dx^2}.\end{aligned} \tag{33}$$

We assume that stress carried by the structure is "σ_0." Hence, the equilibrium equation on every section can be expressed as follows:

$$t_1\overline{\sigma}_x^{(1)} + t_2\overline{\sigma}_x^{(2)} = t_1\sigma_0. \tag{34}$$

Finally, (33) can be rewritten using the above equation as follows:

$$\frac{d^2\overline{\sigma}_x^{(1)}}{dx^2} - \beta^2\overline{\sigma}_x^{(1)} = s(x), \tag{35}$$

where $\beta^2 = (1/X)[2(t_2G^{(3)} + t_3G^{(1)})E^{(3)}/t_1G^{(3)} + t_2E^{(1)}/t_3]$,

$$\begin{aligned}s(x) &= -\frac{t_2E^{(1)}}{t_1X}\sigma_0\\ &\quad + \left[\frac{1}{t_1} - \frac{2\left(t_2G^{(3)} + t_3G^{(2)}\right)E^{(1)}E^{(3)}}{3G^{(1)}G^{(3)}X}\right]\frac{d^2\vartheta_s^{(1)}}{dx^2}\\ &\quad - \frac{t_2t_3E^{(1)}E^{(3)}}{3t_1G^{(3)}X}\frac{d^2\vartheta_s^{(2)}}{dx^2},\end{aligned} \tag{36}$$

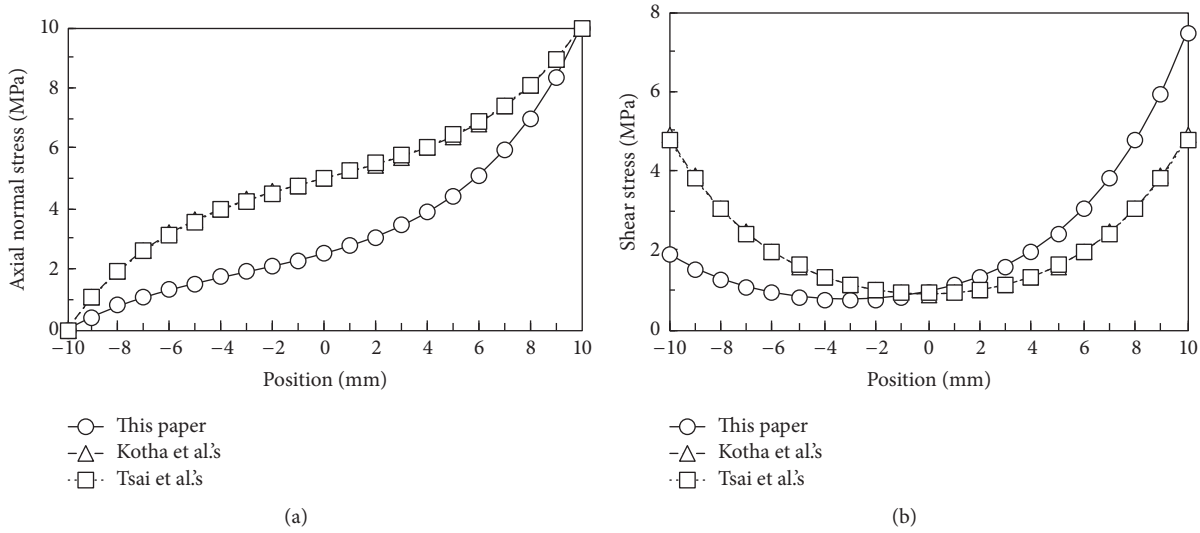

Figure 2: Axial normal and shear stresses ($t_1 = 4\,\mu$m, $t_2 = 150$ nm, $E^{(1)} = 69$ GPa, $E^{(2)} = 3.17$ GPa, $G^{(1)} = 27.6$ GPa, $G^{(2)} = 1.19$ GPa, $\sigma_0 = 10$ MPa).

where $s(x)$ is related to stress at the ends and interfaces. Equation (35) is a normal stress dominant governing equation of layer 1 and uses the boundary conditions at the ends of the structure; the solution of (35) can then be obtained. Shear stress distribution can be obtained by substituting the solution to (9), (10), (27), and (28).

2.2. Results and Discussion. The influence of the surface effect of nanoscale interlayers on stress transfer is quantitatively illustrated by a few examples. Equation (35) is a periodic second-order linear differential equation. For stretched structures, (35) has the same general solution. The complete solution depends on a particular solution, which determines the stress distribution of the structure with different residual interface tensions. Specially, stress transfer is changed by the tangential stress jump at the interface of the interlayer, demonstrating the surface effects. For simplicity, we assume that the geometry and material properties of layers 1 and 3 are the same (i.e., $t_1 = t_3$, $E^{(1)} = E^{(3)}$, and $G^{(1)} = G^{(3)}$). Stress transfer in simple sandwich laminate structure has been analyzed by Kamat et al. and Nairn and Mendels (see [1, 6]) based on shear-lag mode without consideration of surface effects. The relevant material properties are adopted in our manuscript, $E^{(1)} = 69$ GPa, $E^{(1)} = 3.71$ GPa, $G^{(1)} = 27.6$ GPa, $G^{(2)} = 1.19$ GPa, $v^{(1)} = 0.25$, $v^{(1)} = 0.33$. The applied pressure is 10 MPa. For the determination of surface effects, the geometries of interlayers and hard layers are decreased, $l = 20$ mm, $t_1 = 2\,\mu$m, $t_2 = 150$ nm (these changes have no effects on the forms of stress distribution). The residual interface stress induced initial mismatch between the hard phase and interlayers have strong influence on the natural frequency of microbeams, pullout force of nanofibers, and stress transfer [10, 11]. The influences of the three typical residual interface tension distributions on stress transfer are elucidated as follows:

(1) $\vartheta_s^{(1)} = \vartheta_s^{(2)} = \vartheta_s x + \tau_s$: the influence of the surface effects will not be included in a particular solution, where the interface tension is a linear distribution. The stress distributions of the structure are as follows:

$$\begin{aligned} \overline{\sigma}_x^{(1)} &= A_1 \sinh \beta x + B_1 \cosh \beta x + C_1, \\ \tau_{xy}^{(1)}(y_1) &= A_1 t_1 \beta \cosh \beta x + B_1 t_1 \beta \sinh \beta x, \\ \tau_{xy}^{(2)}(y_1) &= \tau_{xy}^{(1)}(y_1) - \tau_s, \end{aligned} \tag{37}$$

where A_1, B_1, and C_1 are known constants provided in Appendix. The surface effects do not directly influence the normal stress of hard layers. Figure 2 shows the stress distributions of the multilayered structure. The structure is essentially symmetric about $x = 0$ (asymmetric along the thickness direction is allowed) but the mechanical boundary condition is asymmetric at ends. As shown in Figure 2, the normal stress distribution is asymmetric and interfacial shear stress is symmetric along the length direction (x-axis). For the symmetric mechanical boundary condition, the normal stress distribution is symmetric but the zero stress at center of the structure is not certainly reached. One of the distributions is the result of our model, and the other two are calculated through classical shear-lag theory without considering the surface effects. Figure 2(a) shows that the normal stress is smaller and smoother than those calculated using the models of Kotha et al. and Tsai et al. [2, 7]. This difference could be attributed to two reasons: uniform deformation of the interlayer over the thickness direction is assumed in their models but is not necessarily limited in our work; and stress jump across the interface is emphasized in our model. Figure 2(b) shows the shear stress of layer 1. The stress obtained using the models of Kotha et al. and Tsai et al. is

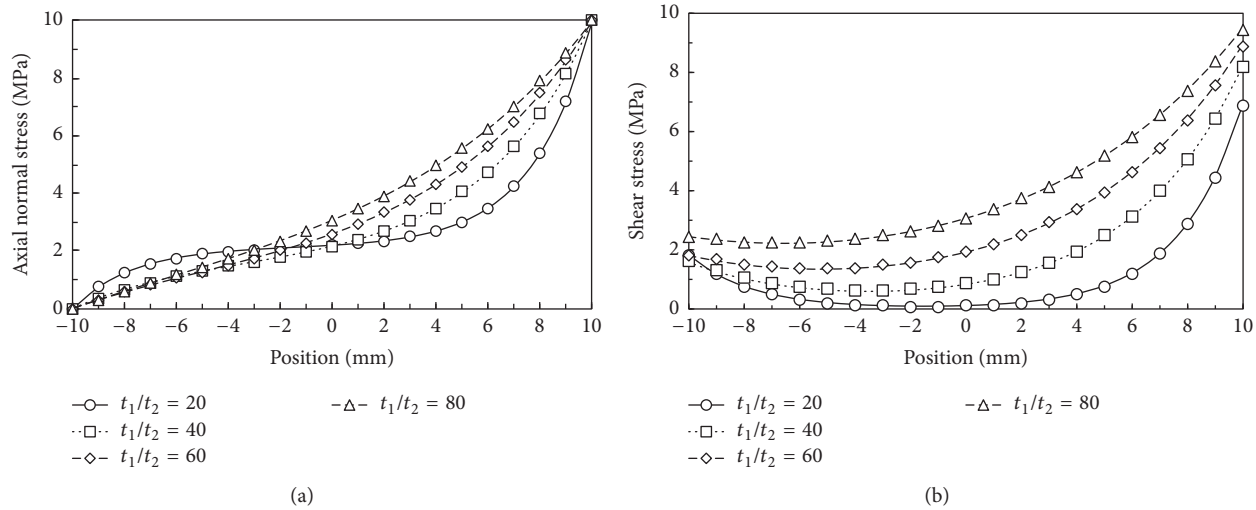

Figure 3: Axial normal and shear stresses along the length of layer 1 with respect to t_1/t_2 ($E^{(1)} = 69$ GPa, $E^{(2)} = 3.17$ GPa, $G^{(1)} = 27.6$ GPa, $G^{(2)} = 1.19$ GPa, $\sigma_0 = 10$ MPa).

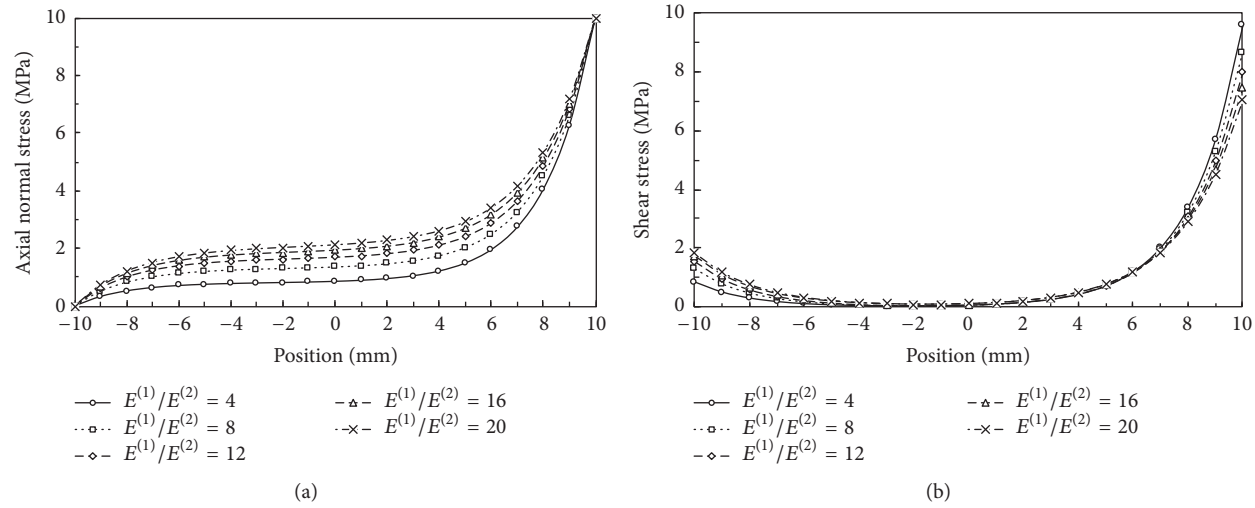

Figure 4: Axial normal and shear stresses along the length of layer 1 with respect to $E^{(1)}/E^{(2)}$ ($t_1 = 4\,\mu$m, $t_2 = 150$ nm, $v^{(1)} = 0.25$, $v^{(2)} = 0.33$, $\sigma_0 = 10$ MPa).

zygomorphic. The calculated result is smaller at the left end and larger at the right end because surface effect increases the efficiency of stress transfer with increasing normal stress. However, the shear stress of the interlayer at the S_1 and S_2 interface differs by a residual surface tension, ϑ_s, compared with the one in layers 1 and 3.

The influence of the geometry and material properties of the interlayer on stress transfer can be studied under linear surface stress distribution. Figure 3(a) shows the plot of normal and shear stress distributions versus the ratio of the thickness of layer 1 to the interlayer. The normal stress in the left region is slightly influenced by the ratio. Accordingly, the transferred stress in the right region increases with decreasing interlayer thickness. The surface effects are enhanced by the nanoscale interlayer. As shown in Figure 3(b), the shear stress also increases with decreasing ratio. Overall, the surface effect influences stress transfer efficiency under the decrease of the interlayer scale. Figure 4 presents the stress distributions of layer 1 versus the ratio of the elastic modulus of layer 1 to that of the interlayer. Similarly, the surface effect definitely increases stress transfer efficiency under the decrease of the interlayer elastic modulus. However, the influence on the shear stress is not significant, except for the right edge (Figure 4(b)).

(2) $\vartheta_s^{(1)} = \vartheta_s^{(2)} = \vartheta_s(x + l/2)(x - l/2)$: the influence of the residual interface tension will appear in a particular solution due to the nonzero second derivative of $s(x)$,

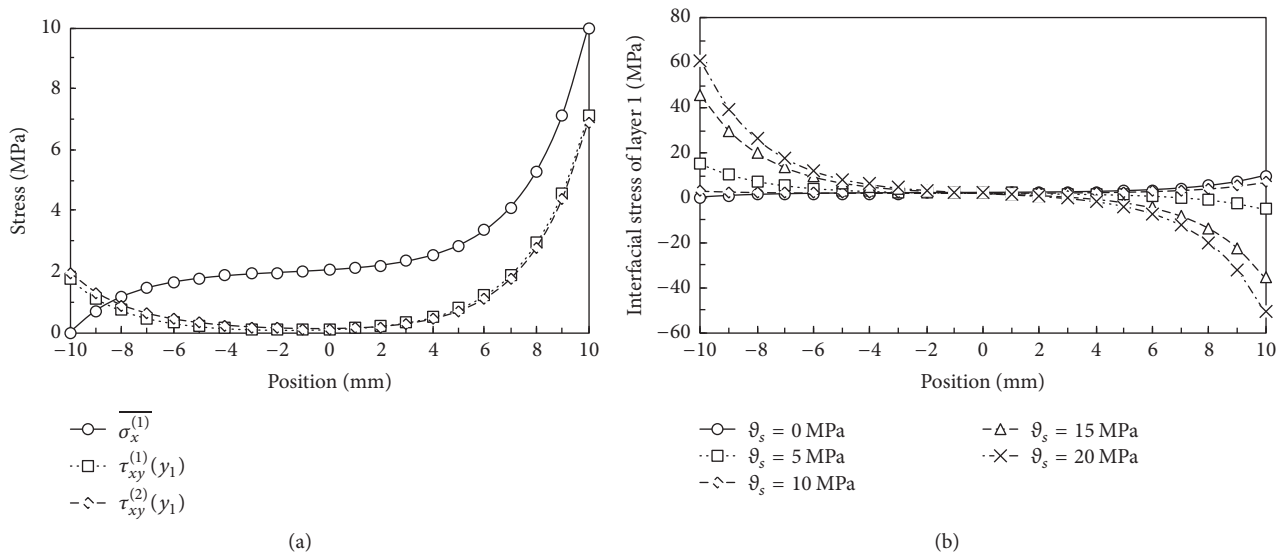

FIGURE 5: Normal and interfacial stresses along the length of layer 1 with parabolic surface tension ($t_1 = 2\,\mu$m, $t_2 = 100$ nm, $E^{(1)} = 100$ GPa, $E^{(2)} = 5$ GPa, $v^{(1)} = 0.25$, $v^{(2)} = 0.33$, $\sigma_0 = 10$ MPa).

where interface tension is a parabolic distribution. The stress distributions of the structure are as follows:

$$\begin{aligned}\overline{\sigma}_x^{(1)} &= A_2 \sinh \beta x + B_2 \cosh \beta x + C_2,\\ \tau_{xy}^{(1)}(y_1) &= A_2 t_1 \beta \cosh \beta x + B_2 t_1 \beta \sinh \beta x,\\ \tau_{xy}^{(2)}(y_1) &= \tau_{xy}^{(1)}(y_1) - 2\vartheta_s x,\end{aligned} \tag{38}$$

where A_2, B_2, and C_2 are known constants and provided in Appendix. The stress transfer of the structure differs from that without the surface effect, where the residual surface stress is a parabolic distribution along the interface. Figure 5 presents the stress distributions. Figure 5(a) shows that the normal stress curve exhibits the same shape with that under the linear surface tension because of the same general solution of (35). The difference in the shear stress of the interlayer at the interfaces and the tangential stress jump is smaller when the residual surface tension amplitude is smaller. Figure 5(b) shows the shear stress distributions versus the tension amplitude of the interlayer. The maximum shear stress at the left and right ends increases with increasing amplitude, except for the central region ($-4\,\text{mm} \le x \le 4\,\text{mm}$). The nonuniform residual surface stress distribution will amplify the influence of the surface effect on stress concentration.

(3) $\vartheta_s^{(1)} = \vartheta_s^{(2)} = \vartheta_s e^x$, $s(x) = \beta_2\sigma_0 + \beta_3 e^x$:

$$\begin{aligned}\overline{\sigma}_x^{(1)} &= A_3 \sinh \beta x + B_3 \cosh \beta x + C_3 e^x + D_3,\\ \tau_{xy}^{(1)}(y_1) &= t_1\left[A_3\beta \cosh \beta x + B_3\beta \sinh \beta x + C_3 e^x\right],\\ \tau_{xy}^{(2)}(y_1) &= \tau_{xy}^{(1)}(y_1) - \vartheta_s e^x,\end{aligned} \tag{39}$$

where β_2, β_3, A_3, B_3, C_3, and D_3 are known constants and provided in Appendix. The surface effect definitely influences the stress transfer when the residual surface stress is an exponential distribution along the interface. Only the shear stress of the interlayer is studied in light of the same general solution and normal stress distribution (Figure 6(a)). Figure 6(b) shows that the shear stress distributions in layer 1 and the interlayer are similar. The difference of the two is also an exponential distribution. The surface effect influence enhances with the transferring distance increase. The shear stress at the interface increases with the surface tension amplitude increase, except for the central region. The larger surface stress distribution will amplify the stress concentration.

3. Conclusions

An improved shear-lag model considering Gurtin–Murdoch elasticity theory is constructed to focus on the stress transfer of nanoscale interlayer with surface effects. The two roles played by the nanoscale interlayer, bounding hard layers, and stress transfer are related to displacement continuity and stress jump at an isotropic interface in this study. For biomaterials, the residual interface tension has a strong influence on the stress transfer of the interlayer. The influences of the three typical residual interface tension distributions on stress transfer are in detail elucidated. The stress distributions of the multilayered structure with the three surface stress situations are obtained. The shear-lag analysis shows that stress transfer of the multilayered structure differs from that of interlayer without the surface effect, where the transferred stress increases with decreasing interlayer thickness and amplified by the surface tension amplitude. Finally, the 2D shear-lag model (see [6]) and interfacial continuity condition

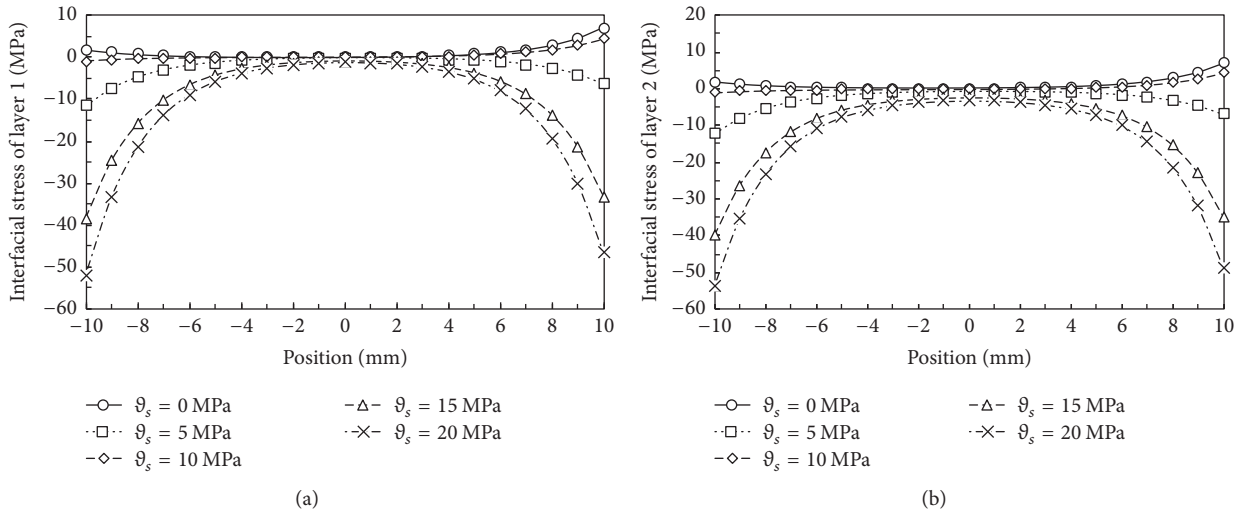

FIGURE 6: Normal and interfacial stresses along the length of layer 1 with exponential surface tension ($t_1 = 2\,\mu$m, $t_2 = 100$ nm, $E^{(1)} = 100$ GPa, $E^{(2)} = 5$ GPa, $\upsilon^{(1)} = 0.25$, $\upsilon^{(2)} = 0.33$, $\sigma_0 = 10$ MPa).

and stress jump can be combined to extend our model's application which may consider the mechanical anisotropy and bending of multilayered structure.

Appendix

For differential (35),

$$\frac{d^2\overline{\sigma}_x^{(1)}}{dx^2} - \beta^2\overline{\sigma}_x^{(1)} = s(x). \tag{A.1}$$

The general solution of the associated homogenous equation is

$$\overline{\sigma}_x^{(1)} = A\sinh\beta x + B\cosh\beta x, \tag{A.2}$$

where A and B are integration constants determined by the following boundary conditions:

$$\begin{aligned}\overline{\sigma}_x^{(1)}\left(x = -\frac{l}{2}\right) &= 0,\\ \overline{\sigma}_x^{(1)}\left(x = \frac{l}{2}\right) &= \sigma_0.\end{aligned} \tag{A.3}$$

The complete solution depends on the distribution of the residual interface tension.

(1) $\vartheta_s^{(1)} = \vartheta_s^{(2)} = \vartheta_s x + \tau_s$, $s(x) = -(t_2E^{(1)}/t_1X)\sigma_0$: the particular and complete solutions are

$$\begin{aligned}\overline{\sigma}_{1x}^* &= \frac{\sigma_0}{1 + 2\left(1 + \left(t_1/t_2\right)\left(G^{(2)}/G^{(1)}\right)\right)},\\ \overline{\sigma}_x^{(1)} &= A_1\sinh\beta x + B_1\cosh\beta x + C_1.\end{aligned} \tag{A.4}$$

The constants are as follows when the boundary conditions (A.2) are used:

$$\begin{aligned}A_1 &= \frac{\sigma_0}{2\sinh\left(\beta l/2\right)},\\ B_1 &= \frac{\sigma_0 - 2\overline{\sigma}_{1x}^*}{2\cosh\left(\beta l/2\right)},\\ C_1 &= \overline{\sigma}_{1x}^*.\end{aligned} \tag{A.5}$$

(2) $\vartheta_s^{(1)} = \vartheta_s^{(2)} = \vartheta_s(x + l/2)(x - l/2)$, $s(x) = (t_2E^{(1)}/\beta^2t_1X)\sigma_0 - (2\vartheta_s/\beta^2)[1/t_1 - (2(t_2G^{(3)} + t_3G^{(2)})E^{(1)^2} + t_2G^{(1)}E^{(1)^2})/3G^{(1)^2}X]$: the particular and complete solutions are

$$\begin{aligned}\overline{\sigma}_{1x}^* &= s(x),\\ \overline{\sigma}_x^{(1)} &= A_2\sinh\beta x + B_2\cosh\beta x + C_2.\end{aligned} \tag{A.6}$$

The constants are as follows when the boundary conditions (A.2) are used:

$$\begin{aligned}A_2 &= \frac{\sigma_0}{2\sinh\left(\beta l/2\right)},\\ B_2 &= \frac{\sigma_0 - 2\overline{\sigma}_{1x}^*}{2\cosh\left(\beta l/2\right)},\\ C_2 &= \overline{\sigma}_{1x}^*.\end{aligned} \tag{A.7}$$

(3) $\vartheta_s^{(1)} = \vartheta_s^{(2)} = \vartheta_s e^x, s(x) = \beta_2\sigma_0 + \beta_3 e^x$ where $\beta_2 = -t_2E^{(1)}/\beta^2t_1X$, $\beta_3 = \vartheta_s[1/t_1 - (2(t_2G^{(3)} + t_3G^{(2)})E^{(1)^2} + t_2G^{(1)}E^{(1)^2})/3G^{(1)^2}X]$: the particular and complete solutions are

$$\begin{aligned}\overline{\sigma}_{1x}^* &= \frac{\beta_3}{1 - \beta^2}e^x - \frac{\beta_2\sigma_0}{\beta^2},\\ \overline{\sigma}_x^{(1)} &= A_3\sinh\beta x + B_3\cosh\beta x + C_3e^x + D_3.\end{aligned} \tag{A.8}$$

The constants are as follows when the boundary conditions (A.2) are used:

$$A_3 = \left(\frac{\sigma_0}{2} - \frac{\beta_3}{1-\beta^2}\sinh\frac{l}{2}\right)\sinh^{-1}\frac{\beta l}{2},$$
$$B_3 = \left(\frac{\sigma_0 + 2\beta_2\sigma_0/\beta^2}{2} - \frac{\beta_3}{1-\beta^2}\cosh\frac{l}{2}\right)\cosh^{-1}\frac{\beta l}{2}, \quad (A.9)$$
$$C_3 = \frac{\beta_3}{1-\beta^2},$$
$$D_3 = -\frac{\beta_2\sigma_0}{\beta^2}.$$

Conflicts of Interest

The authors declare that they have no conflicts of interest.

Acknowledgments

The authors gratefully acknowledge the financial supports to this work from the Natural Science Foundations of China (Grant no. 11272367), the Chunhui Project of Ministry of Education of the People's Republic of China (Grant no. z2014040), the Research Project of Sichuan Provincial Department of Education (Grant no. 15ZA0138), and the Key Research Project of Xihua University (Grant no. z1320608).

References

[1] S. Kamat, X. Su, R. Ballarini, and A. H. Heuer, "Structural basis for the fracture toughness of the shell of the conch Strombus gigas," *Nature*, vol. 405, no. 6790, pp. 1036–1040, 2000.

[2] S. P. Kotha, Y. Li, and N. Guzelsu, "Micromechanical model of nacre tested in tension," *Journal of Materials Science*, vol. 36, no. 8, pp. 2001–2007, 2001.

[3] B. H. Ji and H. J. Gao, "Mechanical properties of nanostructure of biological materials," *Journal of the Mechanics & Physics of Solids*, vol. 52, no. 9, pp. 1963–1990, 2004.

[4] F. Song, J. Zhou, X. Xu, Y. Xu, and Y. Bai, "Effect of a negative poisson ratio in the tension of ceramics," *Physical Review Letters*, vol. 100, no. 24, Article ID 245502, 2008.

[5] A. G. Evans, Z. Suo, R. Z. Wang, I. A. Aksay, M. Y. He, and J. W. Hutchinson, "Model for the robust mechanical behavior of nacre," *Journal of Materials Research*, vol. 16, no. 9, pp. 2475–2482, 2001.

[6] J. A. Nairn and D. A. Mendels, "On the use of planar shear-lag methods for stress-transfer analysis of multilayered composites," *Mechanics of Materials*, vol. 33, no. 6, pp. 335–362, 2001.

[7] M. Y. Tsai, D. W. Oplinger, and J. Morton, "Improved theoretical solutions for adhesive lap joints," *International Journal of Solids & Structures*, vol. 35, no. 12, pp. 1163–1185, 1998.

[8] J. C. Hamilton and W. G. Wolfer, "Theories of surface elasticity for nanoscale objects," *Surface Science*, vol. 603, no. 9, pp. 1284–1291, 2009.

[9] M. E. Gurtin and A. I. Murdoch, "Surface stress in solids," *International Journal of Solids & Structures*, vol. 14, no. 6, pp. 431–440, 1978.

[10] G.-F. Wang and X.-Q. Feng, "Effects of surface elasticity and residual surface tension on the natural frequency of microbeams," *Applied Physics Letters*, vol. 90, no. 23, Article ID 231904, 2007.

[11] B. Gu, H. Zhang, B. Wang, S. Zhang, and X.-Q. Feng, "Mode-I pullout model of nanofibers with surface effects," *Engineering Fracture Mechanics*, vol. 150, pp. 115–125, 2015.

[12] X. L. Fu, G. F. Wang, and X. Q. Feng, "Surface effects on the near-tip stress fields of a mode-II crack," *International Journal of Fracture*, vol. 151, no. 2, pp. 95–106, 2008.

[13] S. Chen and Y. Yao, "Elastic theory of nanomaterials based on surface-energy density," *Journal of Applied Mechanics*, vol. 81, no. 12, Article ID 121002, 2014.

[14] M. Mansfield and R. J. Needs, "Application of the Frenkel-Kontorova model to surface reconstructions," *Journal of Physics: Condensed Matter*, vol. 2, no. 10, article no. 004, pp. 2361–2374, 1990.